Front. Optoelectron. 2015, 8(4): 431–438
DOI 10.1007/s12200-014-0455-x

RESEARCH ARTICLE

Fiber up-taper assisted Mach-Zehnder interferometer for high sensitive temperature sensing

Lili MAO[1,2], Qizhen SUN[1,2], Ping LU (✉)[1,2], Zefeng LAO[3], Deming LIU[1,2]

1 National Engineering Laboratory for Next Generation Internet Access System, Huazhong University of Science and Technology, Wuhan 430074, China
2 College of Optical and electronic information, Huazhong University of Science and Technology, Wuhan 430074, China
3 College of Electrical and electronic Engineering, Huazhong University of Science and Technology, Wuhan 430074, China

Abstract A new in-line Mach-Zehnder interferometer (MZI) sensor consisting of a stub of multi-mode fiber and an up-taper was proposed and demonstrated. Temperature measurement can be carried out by detecting wavelength shift. Dependency of sensitivity on interferometer length and dip wavelength was discussed. Experimental results showed a maximum temperature sensitivity of 113.6 pm/°C can be achieved, which is superior to most fiber temperature sensors based on in-line MZIs within the range from 20°C to 80°C, also a good mechanical strength can be obtained. The proposed sensor is a good candidate for temperature measurement, due to the advantages of simple structure, easy fabrication, cost-effective and high sensitivity.

Keywords fiber sensor, Mach-Zehnder interferometer (MZI), multimode fiber (MMF), up-taper

1 Introduction

Fiber-optic temperature sensors have become increasingly important in various sensing and monitoring applications due to distinctive advantages, such as immunity to electromagnetic interference, lightweight, durability against harsh environments, high sensitivity and resolution [1]. Various fiber-optic temperature sensors have been proposed using different technologies, such as fiber Bragg grating (FBG) [2], long period grating (LPG) [3] and various interferometers including fiber Fabry-Pérot cavities [4–7], Michelson interferometers [8,9], Mach-Zehnder interferometers (MZI) [10–19] and Sagnac interferometer [20–23]. Temperature sensors based on grating need expensive ultraviolet light laser, phase masks, also they suffer from erasing problem under high temperature. Those based on Fabry-Pérot interferometery are usually need expensive femotosecond laser or complicated fabrication process.

For in-fiber MZIs, the extreme simple structure, easy fabrication and low-cost are attractive features among fiber sensors. Many techniques have been proposed by researchers. Jasim et al. [10] presented a temperature sensor through further tapering a microfiber. Nguyen et al. [11] reported a high temperature fiber sensor by splicing a section of single mode fiber (SMF) with two short sections of multimode fibers (MMFs). Lu and Chen [12] demonstrated a femtosecond laser micromachined fiber MZI consists of a micromachined spot cascaded with a taper for sensing. Lu's group [13] also proposed a tapered SMF for simultaneous measurement of refractive index and temperature. Li et al. [14] reported a singlemode-multimode-thinned-singlemode fiber structure for sensing. Wang et al. [15] presented a miniaturized MZI for high-temperature measurement. Geng et al. [16] described an interferometer consists of two concatenated waist-enlarged fusion bitapers. Liu et al. [17] constructed a MZI using a MMF and a tapered SMF. Frazão et al. [18] used a suspended twin-core fiber forming a MZI to discriminate curvature from temperature. The performance of these reported in-fiber MZIs in terms of measured temperature range and maximum sensitivity are listed in Table 1.

In this paper, we report a new in-line MZI sensor consisting of a stub of MMF and an up-taper. Due to the large difference of thermal coefficients between core mode and cladding mode, the proposed interferometer has a high temperature sensitivity of about 113.6 pm/°C, which is higher than reported temperature sensors based on in-fiber MZIs within the range from 20°C to 80°C. Also compared

Received June 19, 2014; accepted September 4, 2014

E-mail: pluriver@mail.hust.edu.cn

Table 1 Comparison of performance of the reported in-line fiber Mach-Zehnder interferometers for temperature sensing

interferometer structure	temperature range/°C	maximum sensitivity /(pm·°C^{-1})	Ref.
microfiber taper	450–802	13.4	[10]
MMF-SMF-MMF	0–900	88	[11]
taper + fs-laser spot	20–100	103	[12]
two taper	20–60	77	[13]
MMF + TF	20–80	61.5	[14]
microcavity	100–1100	46	[15]
two bitaper	25–400	70	[16]
MMF + taper	100–400 400–850	85.8 128.6	[17]
suspended twin-core fiber	10–100	11.4-*x*-axis 2.7-*y*-axis	[18]

Note: TF: thinned fiber

to those in-fiber MZIs based on tapered structures which are fragile for the small taper waist [10,17], here we employed a waist-enlarged up-taper which can get a good mechanical strength. In general, our scheme offers advantages of simple fabrication, low-cost, high sensitivity and enhanced robustness, which are preferable for practical applications.

2 Sensing principle

The proposed structure is fabricated by introducing a section of uncoated SMF2 sandwiched between (MMF and an up-taper, as schematically illustrated in Fig. 1(a). SMF1 and SMF3 are employed as lead-in and lead-out fiber, respectively. Figure 1(b) shows the microscopic image of the up-taper splicing point.

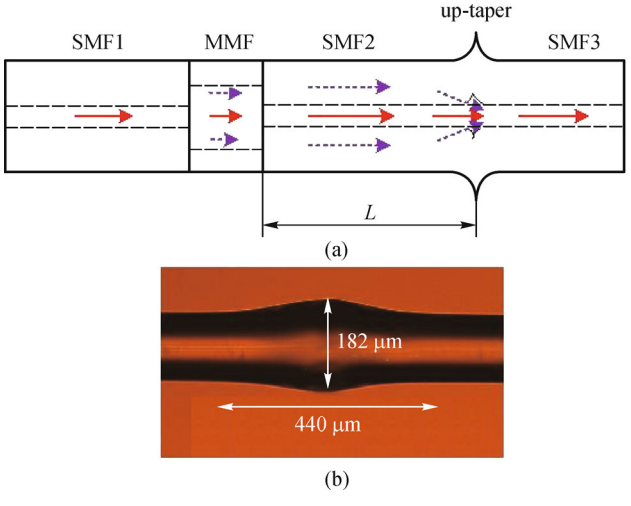

Fig. 1 (a) Structure of a temperature sensor exploiting a section of multimode fiber (MMF) and an up-taper; (b) microscopic image of an up-taper. SMF: single mode fiber

The MMF is only exploited for exciting cladding modes, not for the interference between multiple guiding modes of MMF. So we choose the length of MMF as short as 1 mm in order to reduce the envelope modulation of MMF on the interference pattern.

When the light is launched into MMF through SMF1, multiple guided modes will be excited and propagate in MMF. At the interface between MMF and SMF2, the optical power of core mode is partially coupled into the cladding modes of SMF2 due to the mode field mismatch.

At the up-taper splicing point between SMF2 and SMF3, core mode and part of the cladding modes within SMF2 are coupled into the fundamental mode of SMF3. Resulting from the effective refractive index difference between the core and cladding modes of SMF2, a typical MZI is generated with the intensity as follows [14]:

$$I = I_1 + I_2 + 2\sqrt{I_1 I_2}\cos\left(\frac{2\pi\Delta n_{\text{eff}}^{m} L}{\lambda}\right), \tag{1}$$

where I_1 and I_2 are the optical power of core mode and mth cladding mode participating in the modal interference, respectively. λ is the operating wavelength. $\Delta n_{\text{eff}}^{m} = n_{\text{eff}}^{\text{co}} - n_{\text{eff}}^{\text{cl},m}$ is the effective refractive index difference between the core mode ($n_{\text{eff}}^{\text{co}}$) and the mth cladding mode ($n_{\text{eff}}^{\text{cl},m}$). It should be noted that although many cladding modes are excited in the SMF2, we only consider the dominant cladding mode participated in interference process.

Then we can calculate the resonant dip wavelength of the interference pattern from the following equation:

$$\frac{2\pi\Delta n_{\text{eff}}^{m} L}{\lambda_{\text{res}}} = (2m+1)\pi, \tag{2}$$

where m is a positive integer representing interferential order. Hence, the resonance wavelength λ_{res} can be written as

$$\lambda_{\text{res}} = \frac{2(n_{\text{eff}}^{\text{co}} - n_{\text{eff}}^{\text{cl},m})L}{2m+1}. \quad (3)$$

Accordingly, the relationship between resonance dip wavelength and temperature variation can be calculated by [9]

$$\frac{\mathrm{d}\lambda_{\text{res}}}{\mathrm{d}T} = \lambda_{\text{res}}\left[\frac{1}{n_{\text{eff}}^{\text{co}} - n_{\text{eff}}^{\text{cl},m}}\left(\frac{\mathrm{d}n_{\text{eff}}^{\text{co}}}{\mathrm{d}T} - \frac{\mathrm{d}n_{\text{eff}}^{\text{cl},m}}{\mathrm{d}T}\right) + \frac{1}{L}\frac{\mathrm{d}L}{\mathrm{d}T}\right]. \quad (4)$$

The second term in Eq. (4), $\frac{1}{L}\frac{\mathrm{d}L}{\mathrm{d}T}$, is thermo-expansion coefficient of the silica fiber with a value of about 5.5×10^{-7} °C^{-1}. Thermo-optic coefficient of the Ge-doped silica fiber core is higher (8.6×10^{-6} °C^{-1}) than that of the cladding consisting of fused silica (7.8×10^{-6} °C^{-1}) [12], consequently the effective refractive index of the core mode changes more than that of the cladding mode for the same temperature variation. Then we can get that the wavelength of interference dip λ_{res} will shift to longer wavelength when temperature increases

3 Experiment results and discussion

3.1 Sensor fabrication

In the experiment, the SMFs and MMF we employed has a core/cladding diameter of 9.2/125 μm and 105/125 μm, respectively. The numerical aperture of MMF is 0.26. A stub of MMF is first spliced to a standard SMF1 using a conventional fiber splicer (Fujikura FSM-60S). Then the length of MMF is cut to 1 mm by a highly precise cleaver, and consequently spliced to SMF2. For fabricating the up-taper, the other end of the SMF2 is spliced to SMF3 with a manual operation program. A large "overlap" of 150 μm is chosen for fusion splicing and other parameters (such as arc power, duration time, etc.) are set as default values. Due to the large overlap and pushing force, a waist-enlarged fiber up-taper is fabricated. Figure 1(b) shows the microscopic image of the produced up-taper. The enlarged waist diameter and up-taper length are measured to be around 182 and 440 μm, respectively.

For comparison, we fabricate three interferometers with the same waist diameter (up-taper) and different interferometer lengths (L) ranging from 30 to 50 mm, the interference spectra of these MZIs are shown in Fig. 2.

It can be seen that interferometers with a longer length has a smaller free spectrum range (FSR). Inhomogeneous interference fringes in Fig. 2 indicate that multiple cladding modes participate in interference process. To investigate the number and power distribution of cladding modes contributing in the interference, the transmission spectrum is fast Fourier transformed to get its spatial frequency, as shown in Fig. 3. It is obvious that the power is primarily distributed in the core mode (corresponding to zero frequency) and a dominant cladding mode, which is consistent with aforementioned theoretical analysis. The peak amplitudes of the dominant cladding mode are located at the frequencies of 0.0444, 0.0556 and 0.0887 nm^{-1} for the MZ interferometers with L = 30, 40, 50 mm, respectively. Meanwhile, some other cladding modes corresponding to minor frequency peaks are also excited, but they exhibit weak impact on the interference pattern for low intensities.

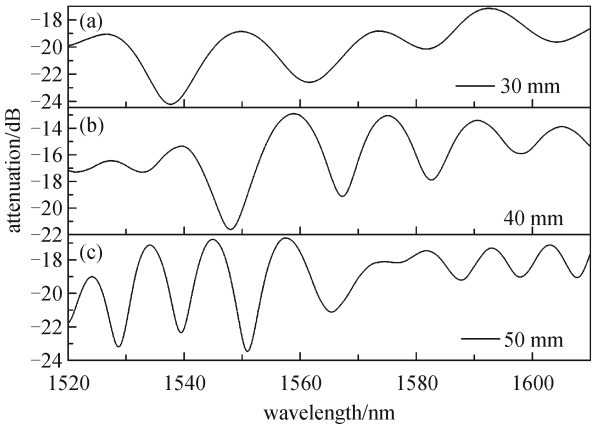

Fig. 2 Normalized transmission spectra for proposed temperature sensor with different interference lengths of (a) 30 mm, (b) 40 mm and (c) 50 mm

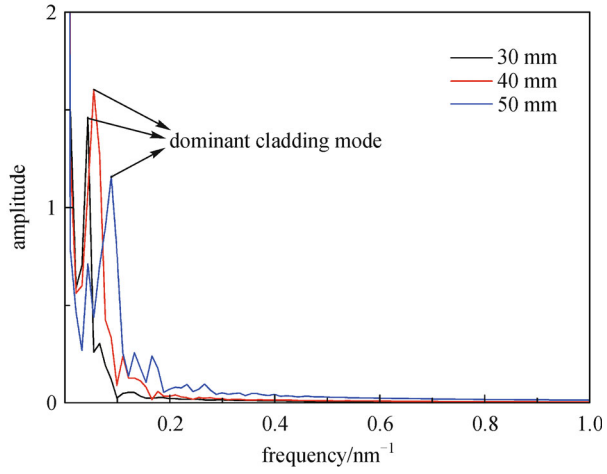

Fig. 3 Spatial frequency spectra of proposed temperature sensor with different interference lengths of 30, 40 and 50 mm

3.2 Experimental setup and temperature measurement

The experimental setup for temperature measurement is displayed in Fig. 4. A broadband light source (BBS) with a wavelength range of 1520–1610 nm is employed to illuminate the sensing fiber. The output spectrum is detected by an optical spectrum analyzer (OSA, YOKOGAWA AQ6370C, Japan). Two ends of the sensor are

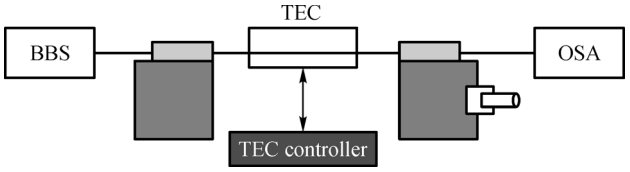

Fig. 4 Experimental setup of a temperature sensor. BBS: broadband light source; TEC: thermoelectric cooler; OSA: optical spectrum analyzer

clamped on high-precision five-dimensional translation stages.

A thermoelectric cooler (TEC) based on Peltier effect is employed to control the temperature change of the sensor with an accuracy of 0.0625°C. The sensor head is heated by a TEC from 20°C to 80°C with a step of 10°C. Measurements are taken every 15 minutes after the temperature stabilized. As the external temperature around the sensor rises, the effective refractive index of the core mode shows a larger change than that of the cladding mode and optical path difference increases accordingly, leading to a red shift of the attenuation dip.

The response to temperature is also tested for the MZI with L = 30, 40 and 50 mm. We take three samples for comparison. Figure 5(a) shows the sensor optical response versus temperature changing from 20°C to 80°C, and Fig. 5(b) shows the dependence of certain dip wavelength shift on temperature for an interferometer with length of 30 mm. Figures 6 and 7 displays the case for 40 and 50 mm length interferometer, respectively.

As shown in Fig. 5(b), for the fiber interferometer of 30 mm in length, if the operation wavelength is selected at 1540 nm (dip A1), the corresponding sensitivities is 64.1 pm/°C. If the operation is selected at 1565 nm (dip B1), the corresponding sensitivity becomes 75.7 pm/°C.

For the 40-, and 50-mm long fiber interferometer at the selected operation wavelength close to 1550 nm, the corresponding sensitivities are 92.4 pm/°C (dip A2) and 78.6 pm/°C (dip A3), respectively, while sensitivities correspond to the wavelength around 1565 nm (dip B2 and dip B3) are 64.3 and 113.6 pm/°C, respectively.

The experimental results show that for both 30 and 50 mm length interferometer, shorter wavelength (around 1550 nm, dip A1 and dip A3) has a smaller sensitivity than longer wavelength (around 1565 nm, dip B1 and dip B3). But it is just the opposite case for 40 mm length interferometer. It can be seen the sensitivity is not monotonously related with dip wavelength. For L = 30 and 50 mm, we can see that with longer length interferometer, which excites cladding mode with higher order (from Fig. 3), accordingly dip A3 possess higher sensitivity than dip A1, so as dip B3 and dip B1. But for

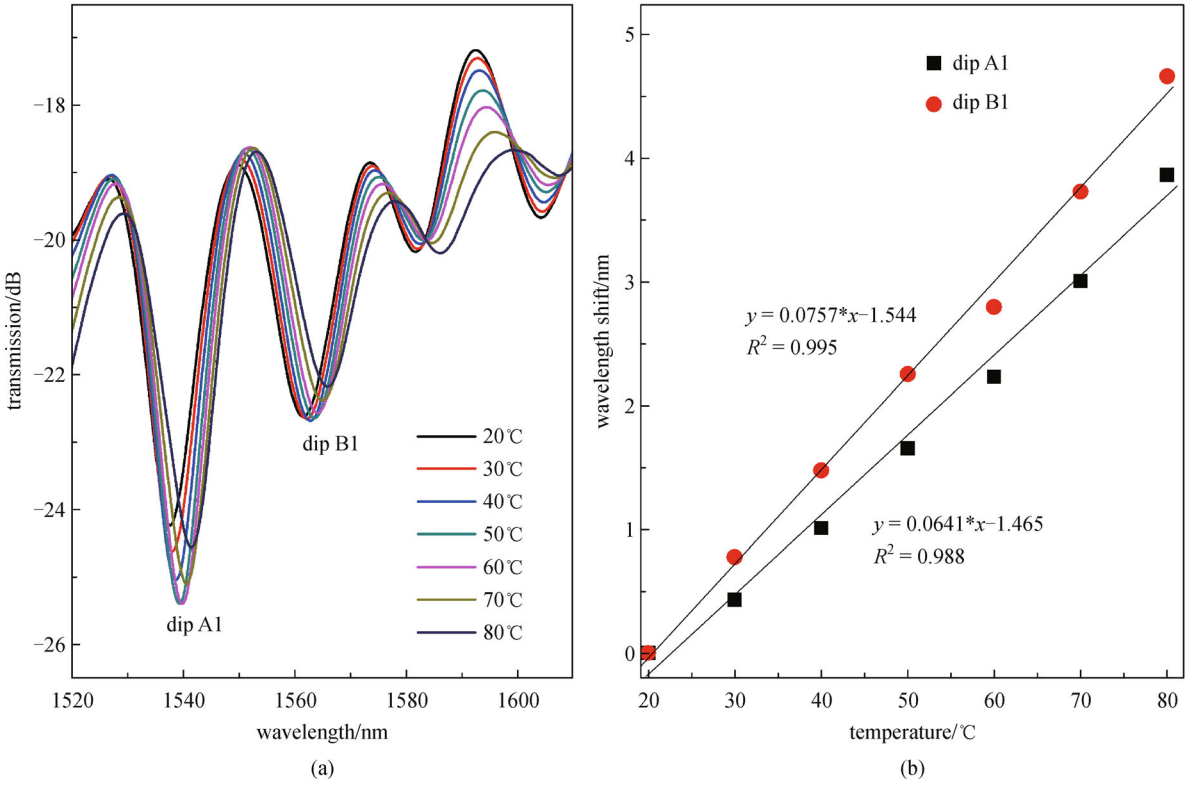

Fig. 5 (a) Transmission spectra of the proposed sensor with a length of 30 mm; (b) relationship between temperature and wavelength shift of resonant dips

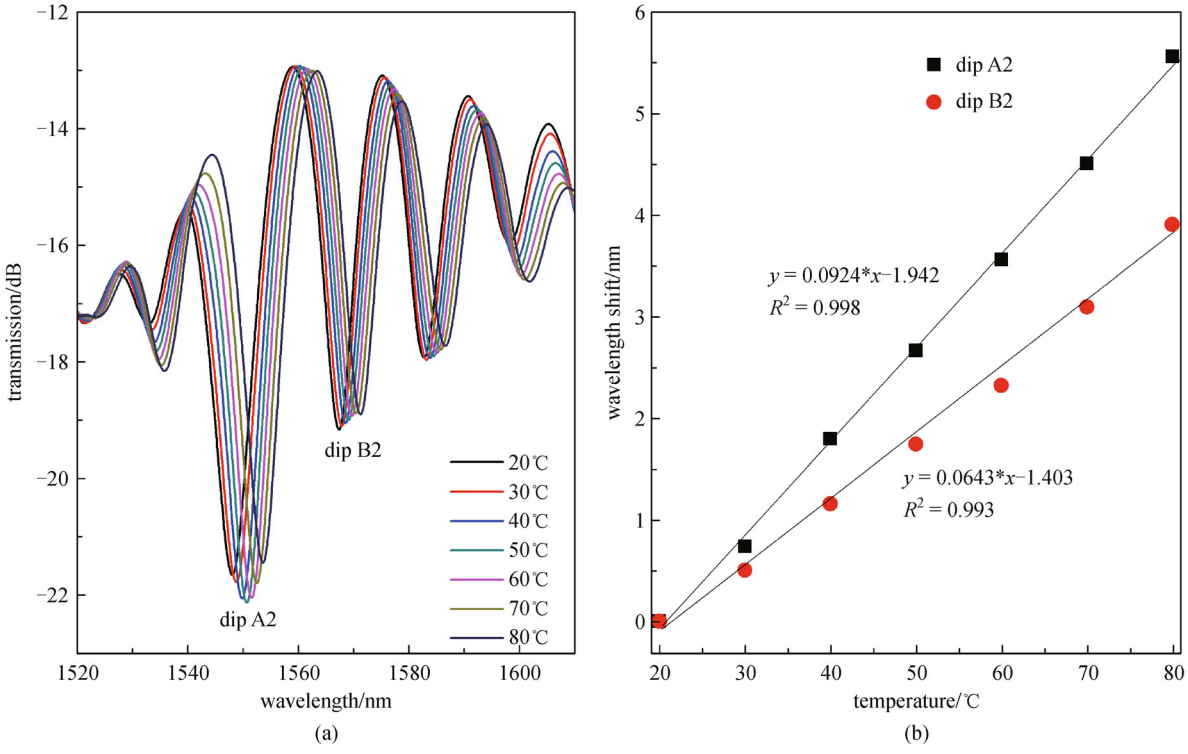

Fig. 6 (a) Transmission spectra of the proposed sensor with a length of 40 mm; (b) relationship between temperature and wavelength shift of resonant dips

the same dip wavelength (1550 nm), longer length interferometer dip A3 has a lower sensitivity than dip B3. This phenomenon is due to different cladding mode participating in the interference with core mode and consequently generating different transmission dips, which exhibits different characteristics. So we can conclude that sensitivity depends on comprehensive effect of many factors, such as dip wavelength, the order of excited cladding mode and length of the interferometer.

It is worth noting that, from Eq. (4), we can also see the sensitivity of our proposed interferometer is related to wavelength (λ_{res}), thermo-optic coefficient ($\mathrm{d}n_{\text{eff}}^{\text{co}}/\mathrm{d}T - \mathrm{d}n_{\text{eff}}^{\text{cl},m}/\mathrm{d}T$) and the coefficient of thermal expansion $\frac{1}{L}\frac{\mathrm{d}L}{\mathrm{d}T}$. It is known that the coefficient of thermal expansion of the fiber is $5.5 \times 10^{-7}\ ^{\circ}\mathrm{C}^{-1}$ [7], which slightly affects the sensitivity of the sensor. So at the same range of wavelength, the sensitivity of the sensor mainly depends on thermo-optic coefficient: $\mathrm{d}n_{\text{eff}}^{\text{co}}/\mathrm{d}T - \mathrm{d}n_{\text{eff}}^{\text{cl},m}/\mathrm{d}T$. The higher order cladding mode has lower thermo-optic coefficient, which will increase the value of $\mathrm{d}n_{\text{eff}}^{\text{co}}/\mathrm{d}T - \mathrm{d}n_{\text{eff}}^{\text{cl},m}/\mathrm{d}T$ [9]. Thus, the relative higher temperature sensitivity of our proposed MZI is due to the higher order cladding mode excitation.

The resolution of optical spectrum analyzer used is 2 pm, so we can get a maximum temperature resolution of 0.0176°C. Due to the limitation of experimental condition, we can only measure temperature less than 80°C, but we believe that our proposed structure can measure higher temperature due to its all-fiber and robust structure.

3.3 Hysteresis test

As the temperature varies in two directions in practical application, it is necessary to investigate the hysteresis of the sensor performance.

As shown in Fig. 8, the red circular dot represents the process of increasing temperature while the blue upward-pointing triangle represents the opposite process. It is obvious that the maximum wavelength shift difference between two directions is 0.06, which is less than 0.87% of the highest wavelength shift. The small error between them may due to the deviation of temperature controlling of the TEC. Also we can get a correlation coefficient of 0.996 between data for two directions.

4 Conclusions

In conclusion, we have demonstrated a new temperature sensor based on MZI employing a stub of MMF and an up-taper. This approach offers an alternative way to detect temperature with a high sensitivity of 113.6 pm/°C, which is higher than most reported in-fiber MZIs within temperature range from 20°C to 80°C. Experimental

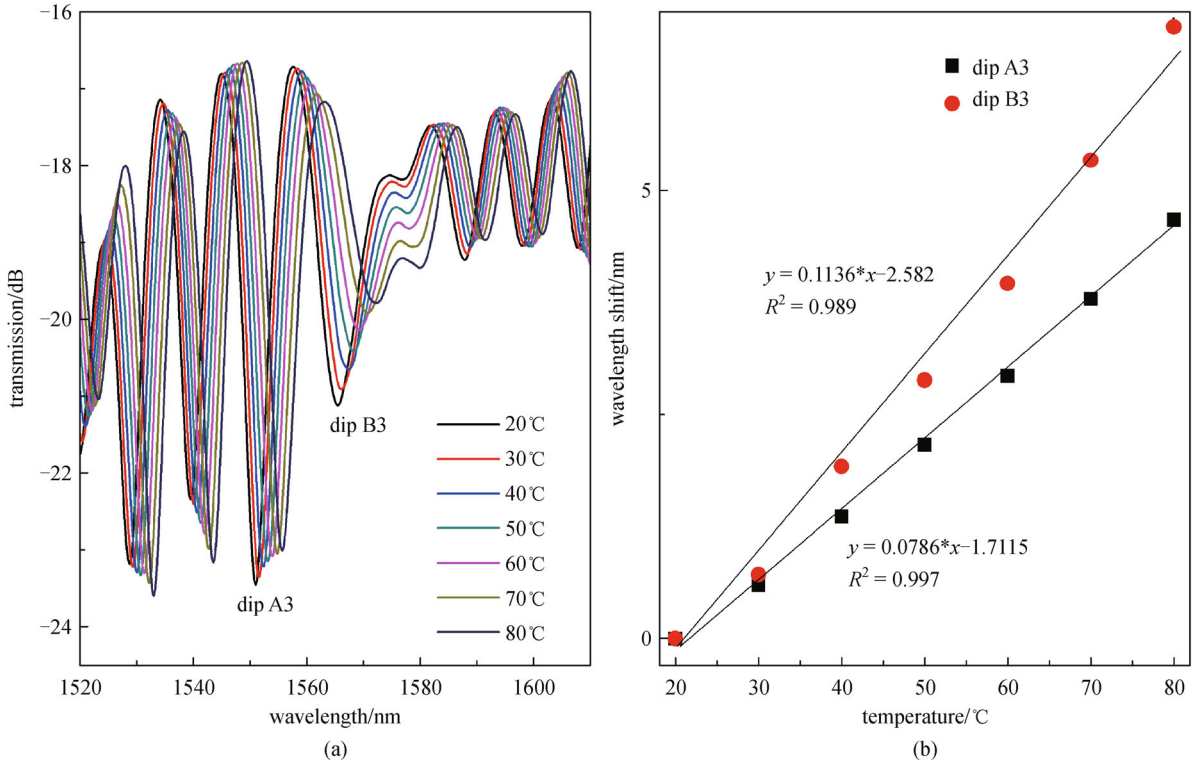

Fig. 7 (a) Transmission spectra of the proposed sensor with a length of 50 mm; (b) relationship between temperature and wavelength shift of resonant dips

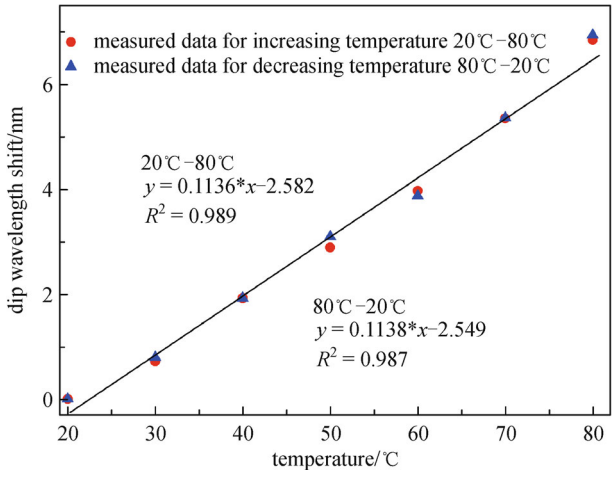

Fig. 8 Relationship between dip wavelength shift and temperature for investigating the repeatability of the experiment

results show hysteresis of less than 0.87% and a good correlation coefficient of 0.996 can be achieved. The advantages include high sensitivity, easy fabrication and low-cost, which can be used for mass-production applications.

Acknowledgements This work was supported by the National Natural Science Foundation of China (Nos. 61275083 and 61290315) and the Fundamental Research Funds for the Central Universities (HUST: No. 2014CG002).

References

1. Li E B. Design and test of multimode interference based optical fiber temperature sensors. Proceedings of the Society for Photo-Instrumentation Engineers, 2008, 7157: 71570F-1–71570F-9
2. Chen C, Yu S H, Yang R, Wang L, Guo J C, Chen Q D, Sun H B. Monitoring thermal effect in femtosecond laser interaction with glass by fiber Bragg grating. Journal of Lightwave Technology, 2011, 29(14): 2126–2130
3. Guo J C, Yu Y S, Zhang X L, Chen C, Yang R, Wang C, Yang R Z, Chen Q D, Sun H B. Compact long-period fiber gratings with resonance at second-order diffraction. IEEE Photonics Technology Letters, 2012, 24(16): 1393–1395
4. Ferreira M S, Coelho L, Schuster K, Kobelke J, Santos J L, Frazão O. Fabry-Pérot cavity based on a diaphragm-free hollow-core silica tube. Optics Letters, 2011, 36(20): 4029–4031
5. Lee C L, Lee L H, Hwang H E, Hsu J M. Highly sensitive air-gap fiber Fabry-Pérot interferometers based on polymer-filled hollow core fibers. IEEE Photonics Technology Letters, 2012, 24(2): 149–151
6. Li X F, Lin S, Liang J X, Zhang Y P, Oigawa H, Ueda T. Fiber-optic temperature sensor based on difference of thermal expansion coefficient between fused silica and metallic material. IEEE

Photonics Journal, 2012, 4(1): 155–162
7. Liu Y, Qu S, Li Y. Single microchannel high-temperature fiber sensor by femtosecond laser-induced water breakdown. Optics Letters, 2013, 38(3): 335–337
8. Li E, Wang X, Zhang C. Fiber-optic temperature sensor based on interference of selective higher-order modes. Applied Physics Letters, 2006, 89(9): 091119
9. Wu D, Zhu T, Liu M. A high temperature sensor based on a peanut-shape structure Michelson interferometer. Optics Communications, 2012, 285(24): 5085–5088
10. Jasim A A, Harun S W, Arof H, Ahmad H. Inline microfiber Mach–Zehnder interferometer for high temperature sensing. IEEE Sensors Journal, 2013, 13(2): 626–628
11. Nguyen L V, Hwang D, Moon S, Moon D S, Chung Y. High temperature fiber sensor with high sensitivity based on core diameter mismatch. Optics Express, 2008, 16(15): 11369–11375
12. Lu P, Chen Q. Femtosecond laser microfabricated fiber Mach-Zehnder interferometer for sensing applications. Optics Letters, 2011, 36(2): 268–270
13. Lu P, Men L, Sooley K, Chen Q Y. Tapered fiber Mach–Zehnder interferometer for simultaneous measurement of refractive index and temperature. Applied Physics Letters, 2009, 94(13): 131110
14. Li L, Xia L, Xie Z, Liu D. All-fiber Mach-Zehnder interferometers for sensing applications. Optics Express, 2012, 20(10): 11109–11120
15. Wang Y, Li Y, Liao C, Wang D N, Yang M, Lu P. High-temperature sensing using miniaturized fiber in-line Mach–Zehnder interferometer. IEEE Photonics Technology Letters, 2010, 22(1): 39–41
16. Geng Y, Li X, Tan X, Deng Y, Yu Y. High-sensitivity Mach-Zehnder interferometric temperature fiber sensor based on a waist-enlarged fusion bitaper. IEEE Sensors Journal, 2011, 11(11): 2891–2894
17. Liu Y, Peng W, Liang Y Z, Zhang X, Zhou X, Pan L. Fiber-optic Mach-Zehnder interferometric sensor for high-sensitivity high temperature measurement. Optics Communications, 2013, 300: 194–198
18. Frazão O, Silva S F O, Viegas J, Baptista J M, Santos J L, Kobelke J, Schuster K. All fiber Mach-Zehnder interferometer based on suspended twin-core fiber. IEEE Photonics Technology Letters, 2010, 22(17): 1300–1302
19. Zhang S, Zhang W, Gao S, Geng P, Xue X. Fiber-optic bending vector sensor based on Mach-Zehnder interferometer exploiting lateral-offset and up-taper. Optics Letters, 2012, 37(21): 4480–4482
20. Zhao C L, Wang Z, Zhang S, Qi L, Zhong C, Zhang Z, Jin S, Guo J, Wei H. Phenomenon in an alcohol not full-filled temperature sensor based on an optical fiber Sagnac interferometer. Optics Letters, 2012, 37(22): 4789–4791
21. Moon D S, Kim B H, Lin A, Sun G, Han Y G, Han W T, Chung Y. The temperature sensitivity of Sagnac loop interferometer based on polarization maintaining side-hole fiber. Optics Express, 2007, 15 (13): 7962–7967
22. Zheng X B, Liu Y G, Wang S, Han T T, Wei C W, Chen J. Transmission and temperature sensing characteristics of a selectively liquid-filled photonic-bandgap-fiber-based Sagnac interferometer. Applied Physics Letters, 2012, 100(14): 141104
23. Han T, Liu Y G, Wang Z, Guo J, Wu Z, Wang S, Li Z, Zhou W. Unique characteristics of a selective-filling photonic crystal fiber Sagnac interferometer and its application as high sensitivity sensor. Optics Express, 2013, 21(1): 122–128

Lili Mao obtained the Master degree in Optoelectronic Information Engineering in 2011 from Huazhong University of Science and Technology, and now is pursuing for the Doctor degree. Her research fields include fiber sensor and fiber laser.

Qizhen Sun received the Doctor degree from Huazhong University of Science and Technology in 2008. She has been an Associate Professor with the College of Optical and Electronic Information, Huazhong University of Science and Technology, since 2011. In 2012, she went to Aston Institute of Photonics Technology as a Visiting Scholar. Her current research interests include fiber-Bragg grating, optical fiber lasers, fiber-optic sensors, and sensor networks.

Ping Lu graduated from Huazhong University of Science and Technology, and obtained the Doctor degree in Electronic Science and Technology. She was promoted to Associate Professor and Professor in 2006 and 2011, respectively, and was engaged in postdoctoral research work in Optical Sciences Center of University of Arizona during 2009—2010. Her research fields include fiber sensor and fiber laser.

Zefeng Lao obtained the Master degree in Electrical Engineering in 2014 from Huazhong University of Science and Technology. His research field is electrical sensor.

Deming Liu received the Doctor degree from Huazhong University of Science and Technology in 1999. He has been a Professor with the College of Optical and Electronic Information, Huazhong University of Science and Technology, since 1994. He was a Visiting Professor with the University of Duisburg-Essen, North Rhine-Westphalia, Germany, from 1994 to

1996, and Nanyang Technological University, Singapore, from 1999 to 2000. Since 2008, he has been the Director of the National Engineering Laboratory for Next Generation Internet Access System. His current research interests include optical access networks, optical communication devices, and fiber-optic sensors.